Stimulus-induced visual cortical networks are recapitulated by spontaneous local and interareal synchronization

Christopher M. Lewis[a,b,1], Conrado A. Bosman[b,c], Thilo Womelsdorf[b], and Pascal Fries[a,b]

[a]Ernst Strüngmann Institute (ESI) for Neuroscience in Cooperation with Max Planck Society, 60528 Frankfurt, Germany; [b]Donders Institute for Brain, Cognition and Behaviour, Radboud University Nijmegen, 6525 EN, Nijmegen, The Netherlands; and [c]Cognitive and Systems Neuroscience Group, Swammerdam Institute for Life Sciences, Center for Neuroscience, University of Amsterdam, 1098 XH, Amsterdam, The Netherlands

Edited by Ranulfo Romo, Universidad Nacional Autonóma de México, Mexico City, D.F., Mexico, and approved December 22, 2015 (received for review July 16, 2015)

Intrinsic covariation of brain activity has been studied across many levels of brain organization. Between visual areas, neuronal activity covaries primarily among portions with similar retinotopic selectivity. We hypothesized that spontaneous interareal coactivation is subserved by neuronal synchronization. We performed simultaneous high-density electrocorticographic recordings across the dorsal aspect of several visual areas in one hemisphere in each of two awake monkeys to investigate spatial patterns of local and interareal synchronization. We show that stimulation-induced patterns of interareal coactivation were reactivated in the absence of stimulation for the visual quadrant covered. Reactivation occurred through both interareal cofluctuation of local activity and interareal phase synchronization. Furthermore, the trial-by-trial covariance of the induced responses recapitulated the pattern of interareal coupling observed during stimulation, i.e., the signal correlation. Reactivation-related synchronization showed distinct peaks in the theta, alpha, and gamma frequency bands. During passive states, this rhythmic reactivation was augmented by specific patterns of arrhythmic correspondence. These results suggest that networks of intrinsic covariation observed at multiple levels and with several recording techniques are related to synchronization and that behavioral state may affect the structure of intrinsic dynamics.

vision | intrinsic activity | oscillations | connectivity | networks

A classical approach to perceptual neuroscience suggests that the brain should respond identically to repetitions of identical stimuli. In this framework, endogenously driven variance in the brain's response to repeated stimuli is considered noise (1). However, this so-called noise has been found to be highly structured and influenced by behavioral context (2). In fact, such variation is a flavor of the ongoing, spontaneous activity of the brain. Both the variation in the brain's response to identical stimuli and its spontaneous activity in the absence of stimulation are endogenously generated and structured in spatially specific intrinsic networks. Highly specific intrinsic networks have been described at essentially all spatial scales: from two individual neurons up to the whole brain. Membrane potentials of nearby neurons show a high degree of spontaneous correlation (3). Neuronal spike rates cofluctuate across physically identical trials, and this so-called noise correlation between neurons is related to the similarity in their stimulus selectivity (4). Correspondingly, when entire maps of population activity are investigated, patterns of activation induced by stimuli are found to reoccur spontaneously (5). The same holds across neighboring maps in auditory cortex, where population activity spontaneously reproduces the tonotopic organization (6). Such coactivations can also be observed with functional MRI (fMRI). In visual cortex, regions selective for either foveal or peripheral stimuli, show correlated blood-oxygen level-dependent (BOLD) activity in anesthetized (7) and resting (8) monkeys. In human subjects, BOLD activity in visual areas is organized into highly specific maps (9–11), the organization of which reflect anatomy (12) and the specificity of which is affected by blindness (13). The finding of robust intrinsic networks using fMRI led to a large number of studies (14), which have recently demonstrated the functional importance of intrinsic networks. For example, spontaneous, correlated BOLD signals predict behavior (15) and relate to learning (16, 17).

Most fMRI studies of intrinsic networks involve interareal correlations, yet we have only a partial understanding of the underlying mechanisms. Recently, it has been shown that interareal BOLD signal correlations between regions of Squirrel monkey somatosensory cortex reflect the somatotopic map and are subserved by millisecond scale spike correlations (18). The rhythmic synchronization of neuronal activity is an interesting candidate mechanism for interareal interactions. Local rhythmic synchronization likely enhances neuronal impact through coincident postsynaptic input (19, 20). Furthermore, interareal rhythmic synchronization aligns temporal windows of excitability and likely renders communication effective (21–23).

We investigate here whether rhythmic synchronization subserves intrinsic networks between visual areas. Using high-resolution multiarea electrocorticography (ECoG) in awake monkeys, and using the retinotopy of early and intermediate visual areas, we show that intrinsic interareal networks recapitulate stimulus induced interareal networks and are subserved by local and interareal synchronization in the theta-, alpha-, and gamma-frequency bands. Surprisingly, even though no clear peaks were evident in

Significance

The greatest proportion of brain activity is endogenously generated. The brain's endogenous activity is highly structured and affects sensory coding, behavior, and perception. The observation of structured endogenous activity across spatial scales suggests that it plays a role in the maintenance and formation of brain networks. The correlation of spontaneous functional MRI signals has demonstrated the existence of multiple intrinsic networks, previously observed during controlled cognitive paradigms. The prevalence and reliability of intrinsic networks have generated intense interest in the functional relevance and electrophysiological basis of interareal correlations. Using multisite recordings from areas V1 and V4 of awake monkeys, we show that endogenously generated activity, both during stimulation and passive fixation, exhibits a similar pattern of local and interareal rhythmic synchronization.

Author contributions: C.M.L., C.A.B., T.W., and P.F. designed research; C.M.L., C.A.B., T.W., and P.F. performed research; C.M.L. analyzed data; and C.M.L. and P.F. wrote the paper with input from C.A.B. and T.W.

The authors declare no conflict of interest.

This article is a PNAS Direct Submission.

Freely available online through the PNAS open access option.

[1]To whom correspondence should be addressed. Email: chris.lewis@esi-frankfurt.de.

This article contains supporting information online at www.pnas.org/lookup/suppl/doi:10.1073/pnas.1513773113/-/DCSupplemental.

power spectra of spontaneous activity, intrinsic networks found in the absence of visual stimulation revealed both arrhythmic and rhythmic processes. Therefore, specific patterns of rhythmic synchronization can exist in power spectra without clear peaks. Further, the emergence of arrhythmic retinotopic coactivation, specifically in passive behavioral states, may indicate a distinct dynamical mode. The results suggest that transitions between behavioral state shape intrinsic networks. Overall, our findings provide a conceptual bridge, linking intrinsic networks to the insights that have been obtained about the biophysical mechanisms underlying rhythmic and arrhythmic synchronization.

Results

We investigated whether intrinsic networks between early (areas V1 and V2) and intermediate (areas V4 and TEO) visual regions are subserved by synchronization. To this end, we obtained measurements of neuronal activity with millisecond temporal resolution and few-millimeter spatial resolution and simultaneous coverage of both cortical regions. We used ECoG in two awake macaque monkeys (monkey P, Fig. 1*A*; monkey K, Fig. S1*A*). For all analyses shown here, the signals from immediately neighboring ECoG electrodes were subtracted from each other to obtain local bipolar derivatives, which are free of the common recording reference, and to which we will refer to as sites. We explored intrinsic networks arising from covariations in local synchrony, i.e., correlated variation of endogenous power between areas, or in interareal synchronization, i.e., coherence between areas. As intrinsic networks can emerge spontaneously, in the absence of stimulation, or as trial-by-trial variation in stimulus-induced responses, we examined the correspondence of the spatial structure of the observed networks to the known spatial structure of visual cortex, namely retinotopy. If the observed intrinsic power covariation or coherence is spatially correlated to retinotopy, it may have a functional role.

Retinotopic Selectivity of ECoG Signals. To assess retinotopic selectivity across all sites of the ECoG grid, monkeys kept fixation for several seconds while visual stimuli were presented randomly interleaved at 60 different positions in the lower right visual quadrant (Fig. 1*B*), corresponding to the portion of visual space covered by our grid. Stimulus position-dependent changes in spectral power (in any frequency band) were established through an ANOVA. The resulting *P* values are shown in Fig. 1*C* (for monkey P; for monkey K, see Fig. S1*B*) and reveal that visually selective sites were mainly found in areas V1/V2 and areas V4/temporal-occipital area (TEO). We selected those sites for further analyses (V1/V2: 68 sites in monkey P, 32 in monkey K; V4/TEO: 17 sites in both monkeys). For these sites, Fig. 1*D* shows how well stimulus position was distinguished based on stimulus-induced power as a function of frequency (both monkeys combined, individual spectra are shown in Fig. S2 *A* and *B*). This plot demonstrates that retinotopic selectivity was present predominantly in a low-frequency band (1–20 Hz) and a gamma-frequency band (60–100 Hz). These two bands also contained the largest stimulus-induced power, as is illustrated in the time–frequency analysis of one example site from area V1 activated by its optimal stimulus (Fig. 1*E* for monkey P; for monkey K, see Fig. S1*C*). This pattern of activity was remarkably consistent across recording sites, stimulus positions, and monkeys (Fig. S2). Although low-frequency activity was present both with and without stimulation, gamma-band activity was primarily stimulus induced, sustained throughout the trial, and had the highest degree of retinotopic selectivity. Low-frequency and gamma-band activity showed distinct poststimulus time courses (Fig. S3 *A, B, E,* and *F*). Gamma-band power was modulated by the phase of low-frequency components, including a strong 2.4-Hz modulation, likely reflecting the stimulus temporal frequency of 1.2 Hz (Fig. S3 *C, D, G,* and *H*). Because gamma-band activity showed the clearest retinotopic selectivity, we illustrate the gamma-band power for all ECoG sites for the same stimulus position in Fig. 1*F* (monkey P; for monkey K, see Fig. S1*D*). The well-localized topographical activation suggests that a given site responds only to a select region of visual space, as was previously shown for these data (24). Indeed, when the site with maximal response in Fig. 1*F* (marked with a star) was selected and the response to all stimulus locations was displayed in Fig. 1*G* (monkey P; for monkey K, see Fig. S1*E*), there was a clearly defined receptive field (RF).

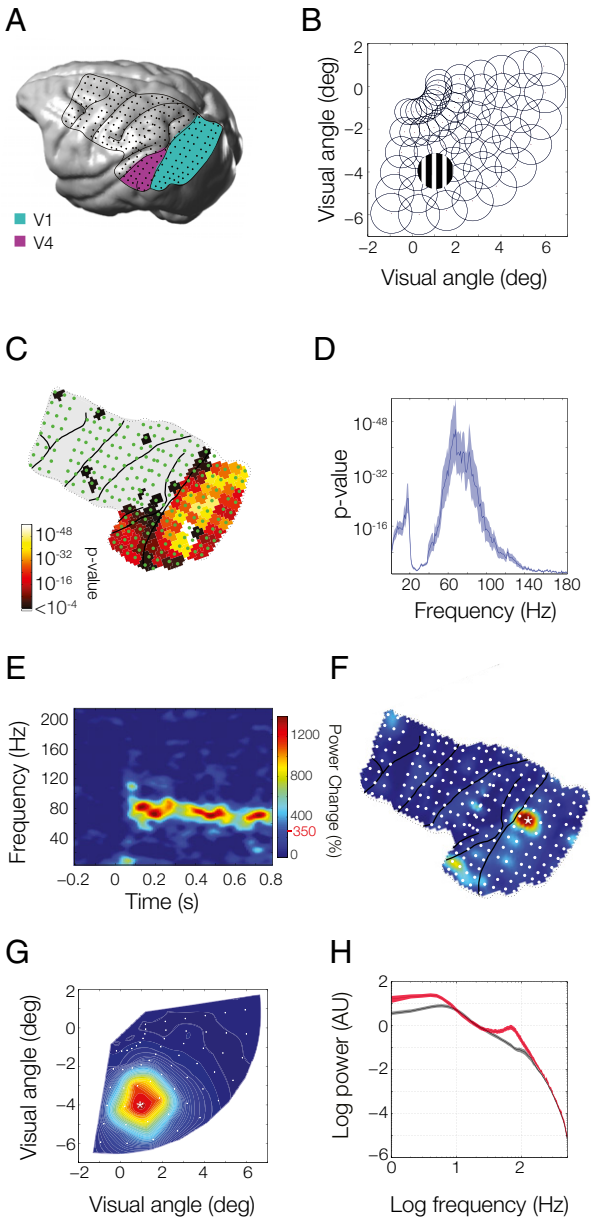

Fig. 1. High-density ECoG layout and receptive field mapping paradigm. (*A*) Rendering of the brain of monkey P with the ECoG grid overlaid. Lines indicate the covered area with the major sulci. Dots indicate the 218 bipolar electrode derivations. Sites considered as lying in areas V1 and V2 are highlighted in green and those in areas V4 and TEO are highlighted in purple. (*B*) Receptive fields were mapped with scrolling gratings at 60 locations in the lower right quadrant, corresponding to the coverage of the ECoG array. (*C*) Selectivity of all ECoG sites for stimulus position based on stimulus induced power in all frequency bands. (*D*) Selectivity of position tuned sites as a function of frequency. (*E–G*) Example average response to stimulation at the position marked in *B*. (*E*) Time-frequency plot at the site marked by a star in *F*. Topographic plot of induced gamma power (80–95 Hz) for each ECoG site. (*G*) Induced gamma band response across all positions for the site marked in *F*. Color bar is the same for *E–G*; red line and value next to color bar indicate significance.

To further investigate the retinotopy of the ECoG recordings from V1, V2, V4, and TEO, we grouped the 60 stimulus locations according to eccentricity or polar angle. Both eccentricity (Fig. 2*E*, monkey P; for monkey K, see Fig. S4*A*) and polar angle (Fig. 2*F* for monkey P; for monkey K, see Fig. S4*B*) were represented in orderly retinotopic maps that corresponded well with previously determined topographies from repeated recordings with penetrating electrodes (25) or from fMRI (26) (Fig. 2 *A*–*D*). Two contiguous maps of space were visible: one behind the lunate sulcus for areas V1/V2 and another one between the lunate and the superior temporal sulcus for areas V4/TEO. For simplicity, we will refer to ECoG sites in the V1/V2 map as V1 and to sites in the V4/TEO map as V4. We investigated whether these maps determined the intrinsic power covariations and/or the coherence between areas. A schematic of our processing stream is displayed in Fig. S5*A*. The main steps are (*i*) quantify the spatial pattern of stimulus-induced power correlation (the covariation of V1–V4 sites by stimulus position); (*ii*) quantify the spatial pattern of intrinsic power correlation or coherence; and (*iii*) Correlate the spatial patterns from *i* and *ii*. As both stimulus-induced (*i*) and intrinsic (*ii*) metrics could be estimated for a full spectrum of frequencies, the correlation (*iii*) could be determined for all pairs of frequencies. To investigate the full pattern of reactivation, we quantified the correspondence between intrinsic synchronization and retinotopy across all frequency pairs. We could therefore document the rich pattern of interareal synchronization in a complete and unbiased manner.

Signal Correlations. To assess the similarity of stimulus preferences between V1 sites and V4 sites, we computed for each interareal site pair the correlation between the average induced power per stimulus position, across the different stimulus positions. Fig. S5*B* shows the gamma band (80–95 Hz) response of a single V1 site to seven repetitions of visual stimulation in four different stimulus positions. The gamma-band response varied systematically as a function of stimulus position in both V1 (Fig. S5*C*) and V4 (Fig. S5*D*), as expected from the results shown in Figs. 1 and 2. It is common (27) to decompose the response to a stimulus into a signal component, considered to be the average response to multiple identical stimulus presentations (black dots in Fig. S5*C* for a V1 site and Fig. S5*D* for a V4 site), and a noise component, considered to be the difference between the average response and the actual response to a particular stimulus presentation (distribution of the gray dots in Fig. S5 *C* and *D* around the black dots). In this framework, the correlation between two sites' average stimulus-induced power across different stimuli is considered the signal correlation (sample site pair shown in Fig. S5*E*), and we will use this term in the following. The signal correlation is calculated per interareal site pair and per frequency band, across the 60 stimulus positions (Fig. S5*G*). The signal correlation captures the similarity of the two sites' stimulus selectivity and therefore reflects the underlying retinotopy. Fig. 3*A* shows the matrix of signal correlations for all possible V1–V4 site pairs for the gamma-frequency band (between 80 and 95 Hz) for monkey P. The repetitive structure in the matrix along both axes reflects the arrangement of electrodes on both areas in distinct lanes, which have been unwrapped along the *x* and *y* axes. This matrix captures the spatial pattern of gamma-band coactivation in V1 and V4 that is due to common drive through stimuli at varying positions.

Fig. 3*B* shows the distributions of signal correlation values across all V1–V4 site pairs as a function of the frequency for which the power was taken. Although specific frequency bands contain most stimulus-related information, signal correlations occur across a broad spectrum of frequencies.

Noise Correlations. As mentioned above, the difference between the average response and the actual response to a given stimulus presentation has been considered noise. Although we believe that this component is not noise, but might reflect sources of uncontrolled endogenous variance, e.g., top-down influences, we will use the signal versus noise terminology for consistency with previous literature. This noise, i.e., the deviations from the average response, has often been found to be correlated across recording sites, i.e., there is noise correlation. We computed noise correlations to assess the degree of power covariation between visual regions that was independent of the stimulus and therefore intrinsically generated (sample site pair, same as above, shown in Fig. S5*F*). The noise correlation is complementary to the signal correlation because, for each pair of recording sites, it captures the intrinsic covariation in power across repeated trials of identical stimulation as opposed to shared stimulus selectivity. Noise correlation was computed for all V1–V4 site pairs and for each frequency (Fig. S5*H*). Fig. 3*C* shows the matrix of noise correlation values from all possible V1–V4 site pairs for the gamma-frequency band (80–95 Hz) for monkey P. This matrix captures the spatial pattern of gamma-band coactivation in V1 and V4 that occurs during stimulation, but reflects intrinsic trial-by-trial variation.

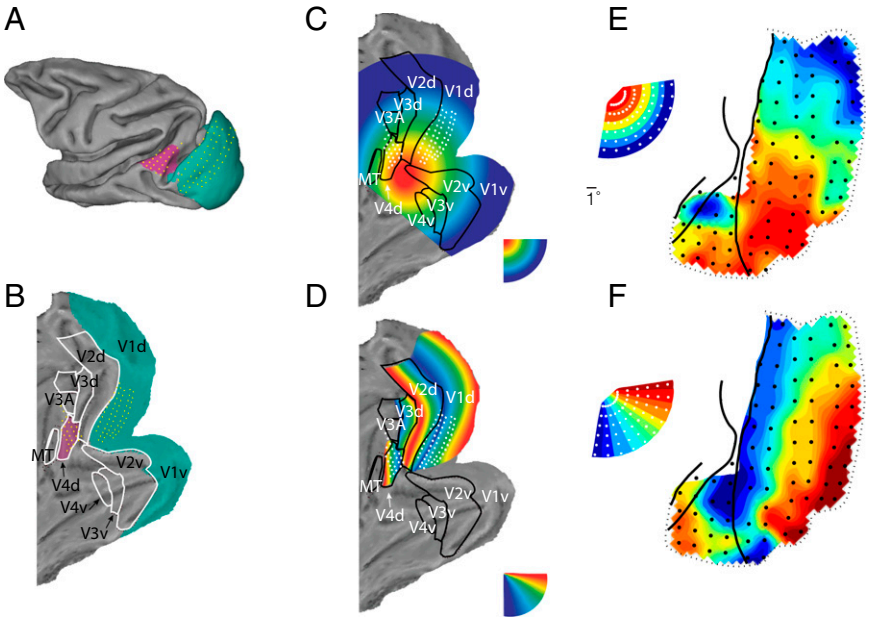

Fig. 2. (*A*) Projection of ECoG electrodes on standard macaque brain [F99 macaque brain from Caret (75)]. (*B*) Same as *A* after unfolding. (*C*) Selectivity for visual stimulus eccentricity, as expected from previous retinotopic mapping studies using penetrating electrodes (25) or fMRI (26). (*D*) Same as *C*, for polar angle. (*E* and *F*) Retinotopic maps based on gamma band (80–95 Hz) activity in monkey P. (*E*) Map of eccentricity; each recording site is colored to indicate the mean eccentricity of the five stimuli giving the largest gamma band response. (*F*) Map of polar angle; each recording site is colored to indicate the mean polar angle as estimated above. *Inset* shows how the 60 stimulus locations are represented across eccentricity and polar angle.

Fig. 3*D* shows the distributions of noise correlation values across all V1–V4 site pairs and reveals similar characteristics as mentioned above for the signal correlations.

Similarity of Noise Correlations to Signal Correlations. To test whether the spatial pattern of noise correlations resembled the spatial pattern of signal correlations, we calculated the correlation between those two metrics, across interareal site pairs. As mentioned above, because both the signal and the noise correlations were determined as a function of frequency, and we considered all possible frequency pairs, this resulted in a frequency-by-frequency matrix of correlation values. We found that noise correlations correlated significantly with signal correlations in specific frequency ranges (Fig. 3*E*). These frequency ranges correspond to those showing the greatest stimulus selectivity (Fig. 1*D*). Thus, interareal power covariations that are extrinsically driven by different visual stimuli are mirrored in power covariations that occur intrinsically in the trial-by-trial variation around the stimulus response, and this effect is most prominent in the frequency ranges with retinotopic selectivity.

The existence of frequency-specific similarity in the spatial pattern of interareal covariation cannot be trivially explained by the pattern of signal correlations. It is possible that noise correlations could occur in an unspecific manner, either spectrally or spatially. For example, on a given trial, all visual channels could have high or low power in a narrow or broad range of frequencies, in which case the degree of noise correlation could be the same as observed, but it would not reflect the underlying retinotopic organization. Such spatially homogenous covariation would be the case if noise correlations reflected unspecific, global, signal variance. However, our results suggest that noise correlations between visual areas obey the functional organization of the underlying cortex.

Similarity of Spontaneous Correlations to Signal Correlations. The signal and noise correlations investigated thus far were derived from the same data, extracting signal-driven variance or endogenous variance and their respective correlation structure. We wondered whether the intrinsically generated covariance resembled the signal correlation also when it was taken from entirely independent data. To this end, we analyzed the fixation periods of separate recording sessions, mostly on different days than the recording sessions analyzed thus far. During these fixation periods, the monkey sat quietly in the booth and fixated a central fixation point while awaiting a different task. We calculated correlations between spontaneous power fluctuations across time after concatenating trials, and we refer to them as spontaneous correlations (Fig. S5 *I* and *J*). Fig. 4*A* shows the spontaneous correlations across the complete matrix of V1–V4 site pairs for the gamma-frequency band in monkey P. Fig. 4*B* shows the distributions of spontaneous correlation values across all V1–V4 site pairs as a function of the frequency for which the power was taken.

Differences in the pattern of correlation for the low- and high-frequency activity were evident in the topographic distribution of spontaneous correlation values. Fig. 4*C* illustrates the spatial pattern for the spontaneous correlation from a seed site in V4 in the 6- to 8-Hz band. The portion of V1 with the highest spontaneous correlation corresponded to the portion with the same retinotopic selectivity as the V4 seed site (*cf* Fig. 2). This retinotopic correspondence held also for spontaneous power fluctuations in the gamma band (80–95 Hz; Fig. 4*D*). Whereas spontaneous correlation values for the theta band were almost exclusively positive, the values for the gamma band were both positive and negative, as expected from Fig. 4*B*.

We found spontaneous correlations to be correlated with signal correlations across V1–V4 site pairs. The retinotopically specific spontaneous coactivation showed a superposition of several correspondences (Fig. 4*E*), specifically (*i*) between spontaneous and signal correlations that were both in either the gamma-band range or the alpha/beta-band range; (*ii*) between signal correlations in the beta band and spontaneous correlations in a very broad band; and (*iii*) between spontaneous correlations in the theta/alpha band and signal correlations in a very broad band. The broadband corre-

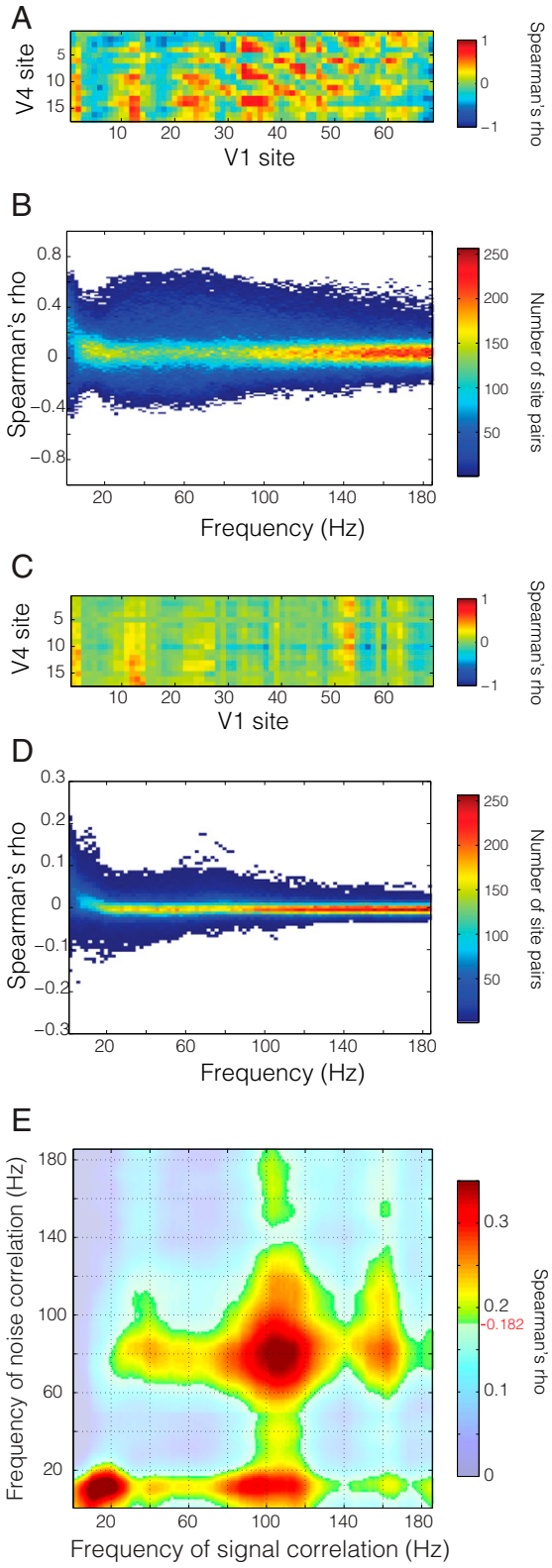

Fig. 3. Signal and noise correlations. (*A*) Signal correlation matrix in the gamma band (80–95 Hz) for all V1–V4 site pairs. (*B*) Distribution of signal correlation values for all interareal site pairs as a function of frequency. (*C*) Noise correlation matrix in the same band as in *A*. (*D*) Distribution of noise correlation values as a function of frequency. (*E*) Correlation of interareal signal and noise correlation matrices (*A* and *C*) across frequencies. Frequency–frequency plane threshold $P < 0.05$ corrected for multiple comparisons. Significance threshold is denoted on color bar by red line and value.

spondences suggest arrhythmic or power-law-like (1/*f*) processes as the underlying source. This superposition of rhythmic and arrhythmic correspondences was revealed through the investigation of the complete frequency-by-frequency plane. By investigating the correspondence between retinotopy and intrinsic signals at all frequency pairs, we were able to uncover important distinctions between passive (Fig. 4*E*) and active (Fig. 3*E*) states. To ensure that the patterns of interareal coactivation we observed were a result of ordered intrinsic activity and not due to fixational eye movements, we computed the correspondence shown in Fig. 4*E* after removing visual sites with parafoveal receptive fields of increasing extent (Fig. S6 *A–F*). This exclusion ensured that fixational eye movements (always ≤1 visual degree) would not lead to the fixation point entering receptive fields and thereby activating neurons. In each analysis, the key points of correspondence between spontaneous correlation and signal correlation remained.

Signal correlations in the gamma band had a similar pattern of correspondence with spontaneous correlations as they had with noise correlations. To demonstrate this similarity, we plot the cross sections showing the correlation spectra for spontaneous and noise correlation with the gamma-range signal correlation (i.e., Figs. 3*E* and 4*E*) in Fig. 4*F*. These cross sections show clear peaks in the delta/theta band and the gamma band. The presence of such peaks for the spontaneous correlation, measured during passive fixation, is in stark contrast to the absolute power spectrum of the local field potential (LFP) during the fixation period, which shows a typical 1/*f* characteristic (Fig. 4*F*, *Inset*). Thus, although there were no appreciable spectral peaks, the spontaneous V1–V4 covariations revealed band-limited processes that were also specifically modulated in the two areas by localized stimuli. In contrast, signal correlations in the alpha/beta band had a different pattern of correspondence with spontaneous correlations versus noise correlations. This difference is demonstrated by corresponding cross sections in Fig. 4*G*. Here, the broadband, arrhythmic component of the spontaneous correspondence diverges from the band-limited low-frequency component, which is present both in the spontaneous correlations and the noise correlations.

Spontaneous Correlations Recapitulate Stimulus Correlations. The retinotopic structure of interareal spontaneous correlations can be demonstrated directly in topographical form, as shown in Fig. 4 *C* and *D*. To assess the degree of this correspondence, we investigated whether the interareal pattern of spontaneous correlations allowed us to derive an ordered topography from stimulation-free data, similar to the retinotopic map derived from visual stimulation data.

To this end, we grouped sites in V4 into regions of interest (ROIs), when they shared similar selectivity either for eccentricity or for polar angle. We calculated spontaneous correlations between each V4 ROI and all V1 sites, separately for the low- (6–8 Hz) and gamma- (80–95 Hz) frequency bands. We hypothesized that a given ROI, with selectivity for either a particular eccentricity or polar angle would show strongest spontaneous correlation with V1 sites sharing the same stimulus selectivity. We indeed found this to be the case. We colored each V1 site according to the eccentricity (Fig. 5 *A* and *C* shows the maps for power in the 6- to 8- and 80- to 95-Hz bands, respectively) or polar angle (Fig. 5 *B* and *D*, as in *A* and *C*) of the V4 ROI to which it showed the strongest spontaneous correlation. To quantify the similarity between these topographies and the retinotopic maps from Fig. 2, we computed the spatial correlation between them. We limited this spatial correlation analysis to sites in V1, because our selection of ROIs in V4 was already based on stimulus preference and so similarities inside V4 were trivial, whereas the pattern seen in V1 was solely the result of topographic specificity of the spontaneous correlations. Both maps derived from spontaneous activity were highly correlated with the retinotopic maps (6- to 8-Hz frequency band: eccentricity map, Spearman's $\rho = 0.366$, false discovery rate across all frequencies, $q < 0.05$; polar angle map, Spearman's $\rho = 0.37$, $q < 0.05$; 80- to 95-Hz frequency band: eccentricity map, Spearman's $\rho = 0.274$, $q < 0.05$; polar angle map, Spearman's $\rho = 0.266$, $q < 0.05$.). Further, when examining the spatial correlation of the maps derived from spontaneous activity with the retinotopic maps across all frequencies (Fig. 5*E*), we again found correspondence specifically in the band below 20 Hz and a broad gamma band between 60 and 150 Hz. These values correspond roughly to the correspondence found through noise correlations, spontaneous correlations, and the frequency bands showing the highest stimulus selectivity. Further, in the spectral region between the two zones of highest correspondence (20–30 Hz), we found some zones of negative correlation, suggesting a different pattern of interareal interaction occurring in this frequency range during spontaneous activity. This finding supports the previous results and further confirms that intrinsic power variations have spatial structure that recapitulates the functional topography of the underlying cortex.

Similarity of Spontaneous Coherence and Directed Influences with Signal Correlation. Given that both noise correlations and spontaneous correlations showed a similar spatial pattern as signal correlations, we asked whether this spatial pattern could also be found in the spontaneous interareal coherence, i.e., in a metric of phase synchronization during spontaneous activity recorded during prestimulus fixation periods. It is possible that the spectral power between areas could be correlated but that the interareal signals would not exhibit a specific phase relationship. For example, rhythmic activity could be generated locally at two locations. The power, or other second-order characteristics, of such locally generated rhythms could be correlated, whereas no first-order dependencies, such as phase coherence, would be present between them. Such a case is particularly plausible in a scenario where the signal power does not depart from a 1/*f* spectrum, suggesting a lack of strong oscillatory activity. Despite this, interareal coherence spectra for the fixation period do demonstrate rhythmic components despite the lack of oscillatory structure in the power (Fig. S7). To our surprise, we found that interareal coherence between visual regions obeyed retinotopic organization in frequency bands similar to those showing similarity in noise correlations and spontaneous correlations (Fig. 6*A*; all spectra are compared in Fig. S8). Thus, even though no clear gamma peak was noticeable in the power spectrum, the correlation analysis revealed that there was spontaneous gamma-band coherence between V1 and V4 that occurred selectively between regions of retinotopic correspondence. As with the spontaneous correlations, derived from periods of passive fixation, the correspondence between spontaneous phase synchronization and retinotopic organization displayed broadband components in addition to band-limited components. Broadband components were mostly between retinotopic organization present in the activity below 20 Hz and spontaneously synchronized broadband activity.

Given that this was the case, we attempted to assess the directionality of the interaction by measuring the granger causal (GC) influences in both directions. We found that signal correlation determined the spatial structure of interareal GC influences both in the direction from V1 to V4 (Fig. 6*B*) and in the direction from V4 to V1 (Fig. 6*C*; interareal granger spectra are shown in Fig. S7).

Discussion

In summary, we found intrinsic networks subserved by local and interareal synchronization, whose spatial structure correlates significantly with stimulus driven patterns of interareal coactivation. Concretely, we found that the spatial structure of signal correlations was recapitulated in (*i*) the trial-to-trial covariability of stimulus induced power (noise correlations), (*ii*) the correlation of spontaneous power fluctuations during fixation (spontaneous correlations), and (*iii*) the spontaneous coherence and GC influences during fixation. We take the specificity of these intrinsically generated patterns of synchronization as a robust indicator of highly organized endogenous activity. Notably, the same spatial pattern of intrinsic covariation was present both during stimulation, i.e., in the noise correlation, and in the absence of stimulation,

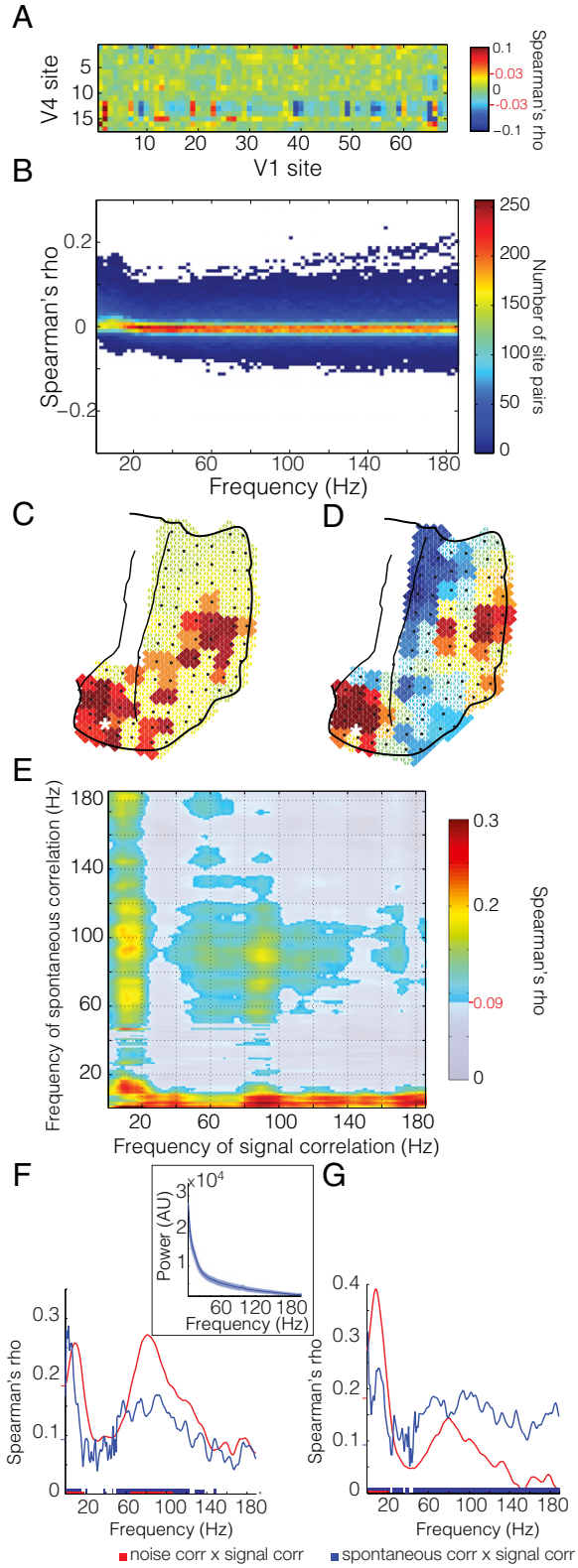

Fig. 4. Spontaneous correlations. (*A*) Spontaneous correlation matrix in the gamma band (80–95 Hz) for all V1–V4 site pairs. (*B*) Distribution of spontaneous correlation values for all interareal site pairs as a function of frequency. Example topographies for spontaneous correlation from the marked V4 site across all visual channels in the (*C*) theta (6–8 Hz) and (*D*) gamma (80–95 Hz) bands (same color bar as *A*). Statistical significance is denoted by red lines and values on color bar, as well as white borders on nonsignificant values in topography. (*E*) Correlation of interareal spontaneous and signal correlation matrices (*A* from Figs. 4 and 5) across frequencies. Frequency–frequency plane threshold $P < 0.05$ corrected for multiple comparisons. Significance threshold is denoted on colorbar by red line and value. (*F*) Comparison of intrinsic correlations with signal correlations for the gamma frequency band (80–100 Hz). The mean correspondences of spontaneous correlation (in blue) and noise correlation (in red) with signal correlation are shown to illustrate their similar spectral profiles. The line spectra are vertical cuts of the respective frequency–frequency plots shown in Figs. 4*E* and 5*E*). Significance threshold at $P < 0.05$ corrected for multiple comparisons, illustrated in blue and red on the *y* axis and significant bands of correspondence illustrated as blue and red bars along the *x* axis. (*Inset*) Spectrum of absolute power of the normalized raw signal (see *Experimental Procedures* for details) for the activity during fixation used to compute spontaneous correlation. Mean across visual sites shown in dark blue. Shaded region denotes SD across sites. (*G*) As in *F*, but for the low-frequency band (1–20 Hz). The mean correspondences of spontaneous correlation (in blue) and noise correlation (in red) with signal correlation are shown to illustrate their different spectral profiles. The line spectra are vertical cuts of the respective frequency–frequency plots shown in Figs. 4*E* and 5*E*). Significance threshold is as explained for *F*.

i.e., in the spontaneous correlation. The patterns present during passive, nonstimulated states were a superset of those present during stimulation (4, 28), suggesting that the intrinsic dynamics may differ between the two states. The presence of rich intrinsic dynamics across states suggests that in addition to the role intrinsic networks may play during passive states, the respective intrinsic networks may influence the pattern of activity during perception and action, and thereby, impact behavior. The temporal structure of the observed intrinsic networks showed both arrhythmic, broadband activity, as well as characteristic frequency bands, corresponding to the rhythms most specifically modulated by visual stimulation, namely the theta, alpha/beta, and gamma rhythms.

One potential concern is that the signal correlation is correlated to intrinsic networks in a spectrally specific way only because the signal correlation itself is spectrally specific to begin with. However, a close examination of the data does not confirm this. For example, Fig. 3*E* shows peaks in the congruence between signal and noise correlation for signal correlations in the frequency bands of roughly 10–20 and 100–120 Hz. Fig. 3*B* shows the distributions of signal correlations and reveals that signal correlations in the 10- to 20-Hz band are among the weakest, and signal correlations in the 100- to 120-Hz band are in the middle of a broad band of all frequencies above 40 Hz, for which the distribution of signal correlations gets progressively narrower. Thus, the frequency bands, in which the signal correlation is particularly congruent to intrinsic correlation patterns, are not particularly conspicuous in the spectral distribution of signal correlation values. Very similar arguments can be made for the congruence between signal correlation and spontaneous correlation, coherence, or GC influences. The frequency bands of highest congruence do not correspond to frequency bands with particularly strong signal correlation. The same reasoning holds for the distributions of noise correlations and spontaneous correlations, which are shown in Figs. 3*D* and 4*B*, and also lack conspicuous structure in the ranges in which they show spatial congruency to the signal correlation. Furthermore, the statistical tests for establishing congruency between signal correlations and intrinsic networks rested on the interareal spatial correlation pattern. By randomizing the spatial relation between interareal sites, we generated surrogate distributions of congruency metrics. Importantly, this randomization left the underlying distribution of the signal correlation unchanged.

The frequency-specific interactions during spontaneous activity occurred in the absence of clear peaks in the LFP power spectrum. This dissociation is noteworthy and requires some explanation. We would like to speculate that local groups of neurons in V1 occasionally show spontaneous epochs of rhythmic synchronization in varying frequency ranges (29). It is possible that the spontaneous epochs of local V1 synchronization cover a broad range of frequencies, similar to stimulus-driven V1 synchronization under variable stimulus or task conditions (23). This vari-

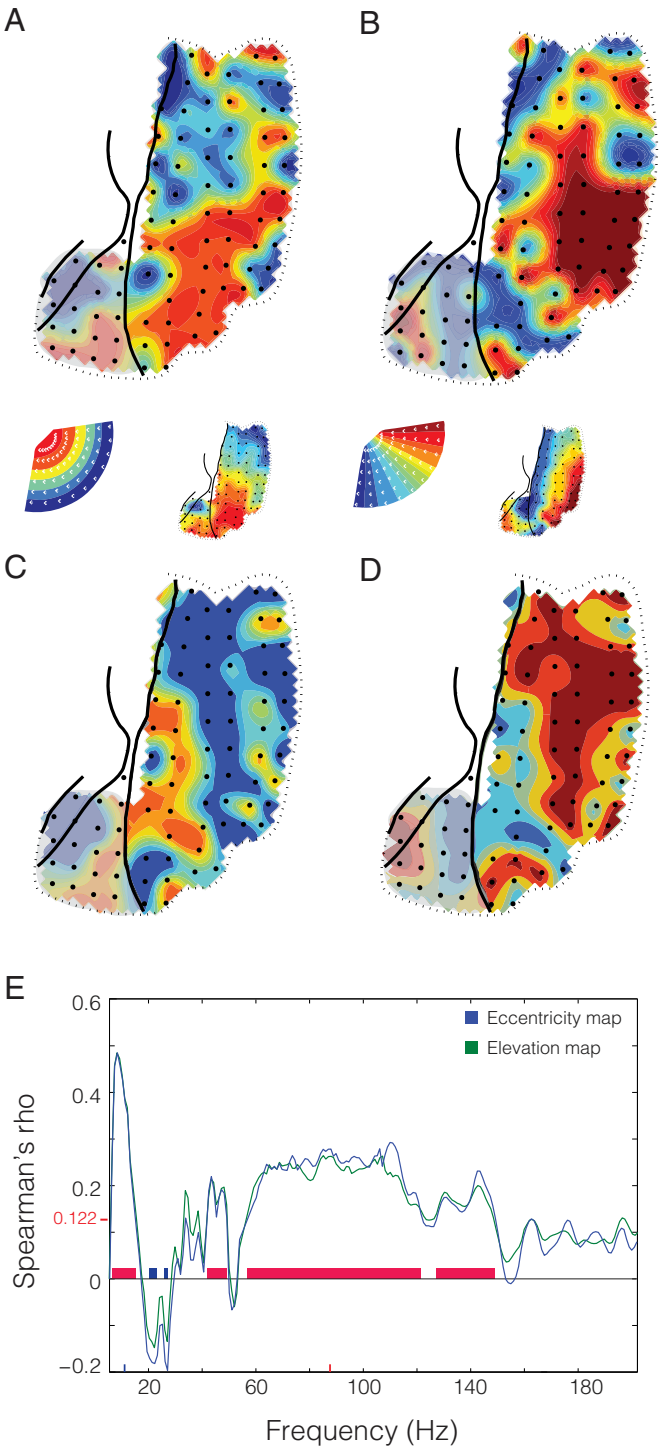

Fig. 5. Retinotopic maps computed from the pattern of spontaneous correlation. (*A* and *C*) Map of eccentricity during passive fixation; each recording site is colored based on the mean eccentricity tuning of the two maximally correlated V4 sites during passive fixation in the (*A*) theta (6–8 Hz) and (*C*) gamma (80–95 Hz) band. (*B* and *D*) Map of polar angle during passive fixation as in *A* and *C*. The retinotopic maps computed from gamma power as in Fig. 2 are shown as *Insets* for comparison. (*E*) Spectrum of spatial correlation values between spontaneous retinotopic maps and stimulus-induced retinotopic maps in area V1. Blue line is for eccentricity; green for polar angle. Significance threshold is denoted on *y* axis by redline and value.

ability in frequency might give rise to a 1/*f* power spectrum (30), and the entrainment of V4 might occur preferentially for certain frequency bands, giving rise to the frequency specificity of the recapitulation. A previous study demonstrated that increasing visual stimulus contrast leads to the peak frequency of local gamma power and interareal coherence to increase over a wide range; intriguingly, the strength of both gamma activity and coherence first increased and then decreased with increasing stimulus contrast (31). If spontaneous activity recapitulates states corresponding to variable stimulus contrasts, these results predict a broad yet defined peak in the gamma-frequency range. Alternatively, the spontaneous epochs of local V1 synchronization occur preferentially in certain frequency bands, which would directly explain the frequency specificity of the recapitulation but would leave the 1/*f* spectrum unexplained. It is conceivable that the power spectrum is less sensitive in revealing rhythmic structure than a correlation spectrum. For example, superimposed 1/*f* noise could mask spectral structure, and the correlation metric could reveal the hidden relationship. We have found before that correlation spectra can sometimes reveal spectral structure, where power spectra do not. We investigated activity recorded from microelectrodes in awake monkey area V4 during fixation in the absence of stimulation (32). LFP power spectra showed a 1/*f* profile, whereas LFP–LFP phase locking spectra and spike–LFP phase locking spectra showed clear gamma peaks (figure S4 and Figure 3 of ref. 32).

Signal correlations showed spatial correspondence with noise correlations mainly for rhythmic components, whereas they showed correspondence with spontaneous correlations for both rhythmic and arrhythmic components. This difference suggests that cortical activity exhibits distinct dynamics during stimulation and in its absence. Although the absence of stimulation might leave cortex to wander through a wider range of dynamical states, the presence of stimulation might constrain this range of dynamic states and thereby produce clear rhythms. In the absence of such stimulus-related constraints, local and short-lived rhythms might well be present, but with variable frequency, strength, and spatial extension. Such passive states would therefore exhibit a characteristic 1/*f* spectrum (33–35). However, nested within an arrhythmic spectrum, highly specific patterns of organization, such as cross-frequency interactions or topographically specific interareal coupling, may reveal specific rhythmic components. Such spontaneously occurring rhythms might couple between V1 and V4 in a retinotopically specific way most strongly, when they occur in particular frequency ranges. The combination of brief epochs of variable frequency and interareal interactions that favor specific frequency ranges could explain why we find broadband correspondences together with correspondences that peak in particular, well-known frequency bands.

Interestingly, the two bands of high correspondence between intrinsic covariation and stimulus driven covariation correspond well with previous findings. Activity in the gamma band is more selective for stimulus properties than oscillations in other bands (36, 37). Furthermore, when natural movies were shown to anesthetized monkeys, most information about the movies was contained in the power time courses of LFP components between 1 and 8 Hz and between 60 and 100 Hz (38). These bands correspond roughly to those in which we find consistency between retinotopy and intrinsic covariation, suggesting that those frequency bands may generally be involved in the representation of visual features within areas and their communication between areas. In fact, within areas, stimulus representation is more accurate for the spikes that are optimally aligned to the gamma rhythm as opposed to spikes that occur at random phases of the gamma cycle (39). Similarly, gamma-band synchronization might facilitate the interareal communication of representations (23): (*i*) interareal gamma phase locking leads to enhanced interareal interactions (22); and (*ii*) the selective interareal communication of attended stimuli is subserved by a corresponding selective interareal gamma-band synchronization (24, 40). Several studies have demonstrated that gamma-band activity is modulated by the phase of lower-frequency components, primarily theta, and this is often referred to as phase-amplitude coupling (PAC) (24,

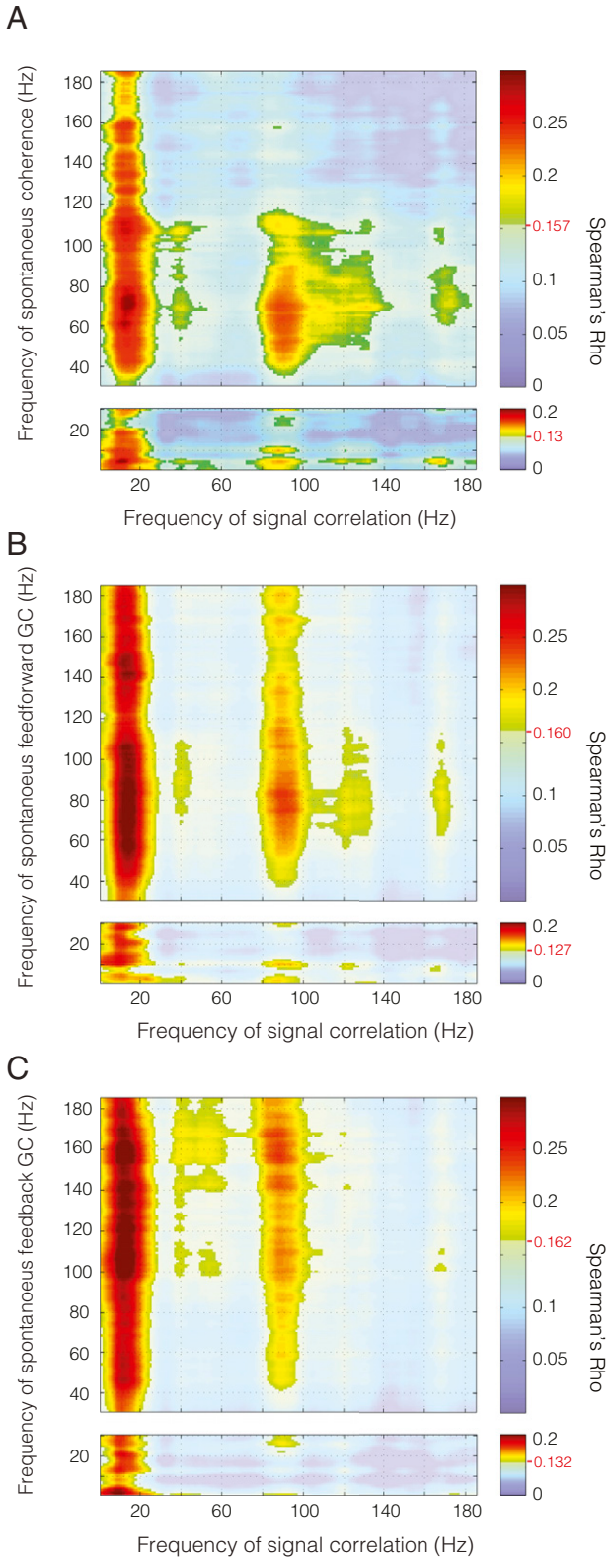

Fig. 6. Spontaneous coherence and directed interaction. Correlation of (*A*) spontaneous coherence, (*B*) spontaneous feed-forward GC, and (*C*) spontaneous feedback GC with signal correlation for all frequencies. Frequency–frequency plane threshold set at $P < 0.05$ corrected for multiple comparisons. Significance threshold is denoted for each comparison by the red line and value on the color bar.

41–44). Local PAC together with interareal low-frequency phase coherence can lead to interareal power-power correlation (45). It will be an interesting topic for future studies to investigate to which degree the patterns of spontaneous recapitulation shown here are due to these mechanisms.

Intrinsic networks defined by structured endogenous activity have been observed at many spatial and temporal scales. Luczak et al. investigated the similarity of stimulus driven and spontaneous patterns of population activity within auditory or somatosensory cortex of both anesthetized and awake rats (4). They found that spike timing patterns were conserved across states of stimulation and spontaneous activity and that the spatial patterns observed during stimulation constitute a subset of all spatial patterns visited by the network during spontaneous activity. Further, they demonstrated the similarity of pairwise correlations between individual cell's firing rates during stimulus driven and spontaneous activity, as well as in noise correlations across repeated stimuli. Similar observations have been made for maps of activity across cat primary visual cortex (5, 46, 47), where activity patterns in the absence of visual stimulation reproduce fine-scale functional organization. Between visual areas, multiple studies have demonstrated retinotopically specific patterns of connectivity across hemispheres in both monkeys and humans (7, 9–11), and human studies have demonstrated differential connectivity within distinct visual pathways (12). Our study helps to link the fine-scale organization of intrinsic activity within areas, with that of the large-scale study of coupling between areas by investigating the fine temporal and spatial dynamics of interareal coupling within the visual system. However, one important caveat of our study is the fact that our ECoG coverage was limited to the dorsal aspect of one hemisphere and to areas in the ventral visual pathway. This limitation constrains the generality of our findings to within-hemisphere connectivity in the ventral visual pathway. Some evidence suggests that our findings may generalize: high-frequency power differentiates tonotopic maps in auditory cortex (6); interhemispheric gamma-band spike synchrony occurs between visual areas dependent of the pattern of stimulation (48); long-range gamma coherence links many visual cortical areas (49), including dorsal visual regions (50) and frontal control regions with ventral visual regions (51); and, finally, spontaneous interhemispheric coupling between auditory areas occurs in the slow covariation of high-frequency power (52).

Electrophysiological correlates of intrinsic networks observed with BOLD are necessary to bridge the gap between detailed accounts of endogenous dynamics within cortical areas to the patterns of activity observed with fMRI across the whole brain. In visual cortex, BOLD signal fluctuations show a positive correlation primarily with LFP power in the gamma-frequency range (53–57). LFP power in the gamma-frequency range can reflect both rhythmic neuronal synchronization at the gamma rhythm (19, 58, 59) and the broadband spectral signature of basic biophysical processes like spikes and/or postsynaptic potentials (60, 61), a distinction that is increasingly made explicit (62). The BOLD signal appears related to both the strength of broadband gamma-range power (55) and the strength of the band-limited gamma rhythm (56, 57). Correspondingly, LFP power in the gamma-frequency range is correlated between corresponding regions of the two hemispheres (52), fluctuates spontaneously according to tonotopic maps in auditory cortex (6), and reflects regional boundaries in somatomotor cortex, in close correspondence to BOLD signal fluctuations (63). When activity in BOLD signal-defined intrinsic networks is directly correlated to EEG band-limited power, distinct networks relate to various frequency bands (64). Conversely, power fluctuations in different frequency bands of the EEG signal are related to distinct spatial patterns of brain activation observed with simultaneous fMRI (65, 66). Power cofluctuations were also demonstrated directly with source-projected magnetoencephalography (MEG), revealing distinct spatial networks for power in different frequency bands (67–69). Related findings have been reported in recordings from cat brain regions homologous with two well-described human fMRI intrinsic

networks: the task-on and task-off networks (70). Between those two networks, total LFP power during spontaneous activity showed an overall difference, and periods in which band-limited power time courses were anticorrelated. In the task-off network, reduced power was surprisingly correlated to enhanced neuronal firing rates, illustrating the importance of combined multilevel investigations.

We showed that intrinsic networks are subserved by specific patterns of synchronization. The pattern of synchronization varies between dominantly narrow-band, rhythmic activity during periods of stimulation and a mixture of both broad- and narrow-band synchronization during periods of spontaneous activity. Rhythmic activity was evident even when the power spectrum exhibited no spectral structure. Rhythmic and arrhythmic activity occurred in distinct portions of the frequency–frequency interactions, suggesting that they occur distinctly within the data. Rhythmic activity was evidenced by clear spectral peaks that exclude broadband power changes as underlying causes and rather correspond to classical frequency bands. Arrhythmic activity was mainly present in the correspondence of intrinsic signals with retinotopic organization below 20 Hz. The segregation of these two modes of activation suggest that broadband activity may be specifically modulated by low-frequency activity, as has been demonstrated in human ECoG recordings (42, 71). The rhythmic activation of particular interest occurred in the gamma-frequency band and has been linked to interareal communication. Communication is likely supported by gamma-band coherence. Surprisingly, gamma-band coherence, normally observed exclusively during stimulation, was found in spontaneous activity to reflect the spatial pattern of signal correlations. This finding provides a potential link from the putative mechanism of communication through coherence to the organization of endogenous activity in intrinsic networks. The link could be shown due to ECoG recordings that combined high temporal and high spatial resolution with coverage of two visual areas. The high temporal resolution was necessary to reveal the spectral specificities, the high spatial resolution enabled topographic specificity, and the coverage was required to allow the interareal correlation between spatial patterns of spontaneous and stimulus-driven activity. It will be an intriguing possibility for future research to capitalize on these features and investigate whether, e.g., the influence of intrinsic networks on stimulus responses or behavior is spectrally specific or whether experience shapes the dynamics of intrinsic networks in particular frequency bands. Furthermore, it will be crucial to extend coverage to both hemispheres to allow investigation of bilateral symmetric patterns, which have been the hallmark of many fMRI demonstrations of intrinsic networks, and finally to add single cell recordings that will allow the integration of population dynamics into large-scale patterns.

Experimental Procedures

Neurophysiological Recording Techniques and Signal Preprocessing. All procedures were approved by the ethics committee of the Radboud University (Nijmegen, The Netherlands). The data used for the analysis presented in this manuscript are available to interested parties by contacting the authors. More information is provided in *SI Experimental Procedures*.

Visual Stimulation. Stimuli and behavior were controlled by the software CORTEX. More information is provided in *SI Experimental Procedures*.

Data Analysis General. All analyses were performed in MATLAB (MathWorks) using FieldTrip (72) (www.fieldtriptoolbox.org). More information is provided in *SI Experimental Procedures*.

Retinotopic Maps. To construct retinotopic maps for eccentricity and polar angle, the mean power was computed across trials for each stimulus location. First, each trial was cut to the time between 0.3 s after stimulus onset (to avoid the early transient activity) and 0.9 s. Frequency analysis was performed by computing the fast Fourier transform of the entire stimulation epoch. Each site was assigned an eccentricity and a polar angle based on the position of the stimulus giving the maximal response in the gamma band. The overall pattern of retinotopic organization was robust to different manners of computing the preferred eccentricity and polar angle and so the maximal stimulus was chosen because of its simplicity.

Signal and Noise Correlations. To compare the spatial patterns of stimulus-driven correlations and stimulus-independent correlations, frequency-resolved signal and noise correlations were computed. Signal correlation was computed by first calculating the mean spectral responses per stimulus position, across trials, and then determining the Spearman rank correlation across the mean stimulus responses, between interareal site pairs. Noise correlation was computed by first calculating the trial-by-trial deviation from the mean response for each condition and then determining the Spearman rank correlation across trials between interareal site pairs. Noise correlations were computed independently for each stimulus position and then averaged across conditions to avoid any modulation by stimulus preference from contaminating the results. Across all interareal site pairs, we then calculated the Spearman rank correlation between signal correlations and noise correlations. The Spearman rank correlation was used to avoid assumptions about underlying distributions. However, results were essentially the same when Pearson correlation coefficients were used.

Spontaneous Correlation. For the analysis of spontaneous activity, we used the period of passive fixation during an attention task, which contained stimuli at two fixed positions, one of them contralateral to the recorded left hemisphere. Recordings during the attention task occurred in different sessions and often on different days than retinotopic mapping. We defined fixation as the time period from 0.3 s after fixation point onset and after the monkey acquired fixation until 0.1 s before the first stimulus appeared on the screen. As with signal and noise correlations, spontaneous correlations during fixation where computed for each frequency of interest and for each channel pair.

Spontaneous Retinotopy. Retinotopic maps were computed during passive fixation by first determining the eccentricity and polar angle preference of recording sites in V4. Once this was determined, V4 sites were grouped into ROIs with similar eccentricity (6 ROIs) or polar angle preference (10 ROIs). For each ROI, average time series of band-limited power were computed and correlated separately with power time courses of each V1 site. This analysis resulted in 6 V1 maps of correlation for eccentricity and 10 maps of correlation for polar angle. To compute the topography in V1 during the period of spontaneous activity, each recording site in V1 was assigned the value of the retinotopic preference of the V4 ROI it was most strongly correlated with. This process resulted in maps of intrinsically generated retinotopy for each frequency of interest. To quantify the extent to which spontaneous retinotopy corresponded with stimulus driven retinotopy in area V1, we computed the spatial correlation of those maps computed during spontaneous activity with stimulus derived retinotopic maps for eccentricity and polar angle.

Spontaneous Coherence and Directed Influence. For the analysis of spontaneous coherence and directed influence, we used the same passive fixation periods as during spontaneous correlation. We computed the coherence and GC using two separate analysis approaches: one for frequencies less than or equal to 30 Hz and the other for frequencies between 31 and 190 Hz. We did this because high-frequency components characteristically have less power and broader spectral bands than low-frequency components. Therefore, it is advantageous to apply different frequency-domain smoothing to these two distinct frequency bands. For both analyses, we cut the fixation data into 500-ms segments and computed the cross-spectral density matrix (CSD) using the fast Fourier transform. In the low-frequency band, we used a Hann taper. For the high-frequency band, we used multitapering with 11 tapers from the discrete prolate spheroid sequence (73), resulting in a spectral smoothing of $\pm$11 Hz. After calculation of the CSD, we either calculated coherence or GC. GC was calculated using nonparametric spectral factorization (74). The pattern of interareal coherence and GC was then correlated with the pattern of stimulus selectivity for each combination of frequencies.

Statistical Testing. Wherever possible, data from both monkeys were combined. The combined results amount to a fixed-effect analysis for our sample of two animals. More information is provided in *SI Experimental Procedures*.

ACKNOWLEDGMENTS. We thank M. Corbetta for discussions during the genesis of this project and R. Oostenveld for assistance in technical matters. This work was supported by Human Frontier Science Program Organization Grant RGP0070/2003 (to P.F.); Volkswagen Foundation Grant I/79876 (to P.F.); a European Young Investigator award (to P.F.); European Union Grant HEALTH-F2-2008-200728 (BrainSynch to P.F. and C.M.L.); the Landes-Offensive zur Entwicklung Wissenschaftlich-ökonomischer Exzellenz ("Neuronale Koordination Forschungsschwerpunkt Frankfurt" to P.F.); the Smart Mix Programme of the Netherlands Ministry of Economic Affairs and the Netherlands Ministry of Education, Culture and Science (BrainGain to P.F. and C.M.L.); the European Commission Seventh Framework Programme (FP7/2007-2013) under Grant 604102 (Human Brain Project; to P.F. and C.M.L.); and The Netherlands Organization for Scientific Research Grants 452-03-344 (to P.F.) and 016-071-079 (to T.W.).

1. Shadlen MN, Newsome WT (1994) Noise, neural codes and cortical organization. *Curr Opin Neurobiol* 4(4):569–579.
2. Cohen MR, Newsome WT (2008) Context-dependent changes in functional circuitry in visual area MT. *Neuron* 60(1):162–173.
3. Lampl I, Reichova I, Ferster D (1999) Synchronous membrane potential fluctuations in neurons of the cat visual cortex. *Neuron* 22(2):361–374.
4. Luczak A, Barthó P, Harris KD (2009) Spontaneous events outline the realm of possible sensory responses in neocortical populations. *Neuron* 62(3):413–425.
5. Kenet T, Bibitchkov D, Tsodyks M, Grinvald A, Arieli A (2003) Spontaneously emerging cortical representations of visual attributes. *Nature* 425(6961):954–956.
6. Fukushima M, Saunders RC, Leopold DA, Mishkin M, Averbeck BB (2012) Spontaneous high-gamma band activity reflects functional organization of auditory cortex in the awake macaque. *Neuron* 74(5):899–910.
7. Vincent JL, et al. (2007) Intrinsic functional architecture in the anaesthetized monkey brain. *Nature* 447(7140):83–86.
8. Belcher AM, et al. (2013) Large-scale brain networks in the awake, truly resting marmoset monkey. *J Neurosci* 33(42):16796–16804.
9. Arcaro MJ, Honey CJ, Mruczek RE, Kastner S, Hasson U (2015) Widespread correlation patterns of fMRI signal across visual cortex reflect eccentricity organization. *eLife* 4: e03952.
10. Heinzle J, Kahnt T, Haynes JD (2011) Topographically specific functional connectivity between visual field maps in the human brain. *Neuroimage* 56(3):1426–1436.
11. Raemaekers M, et al. (2014) Patterns of resting state connectivity in human primary visual cortical areas: A 7T fMRI study. *Neuroimage* 84:911–921.
12. Genç E, Schölvinck ML, Bergmann J, Singer W, Kohler A (August 12, 2015) Functional connectivity patterns of visual cortex reflect its anatomical organization. *Cereb Cortex*, 10.1093/cercor/bhv175.
13. Butt OH, Benson NC, Datta R, Aguirre GK (2013) The fine-scale functional correlation of striate cortex in sighted and blind people. *J Neurosci* 33(41):16209–16219.
14. Fox MD, Raichle ME (2007) Spontaneous fluctuations in brain activity observed with functional magnetic resonance imaging. *Nat Rev Neurosci* 8(9):700–711.
15. Hesselmann G, Kell CA, Kleinschmidt A (2008) Ongoing activity fluctuations in hMT+ bias the perception of coherent visual motion. *J Neurosci* 28(53):14481–14485.
16. Baldassarre A, et al. (2012) Individual variability in functional connectivity predicts performance of a perceptual task. *Proc Natl Acad Sci USA* 109(9):3516–3521.
17. Lewis CM, Baldassarre A, Committeri G, Romani GL, Corbetta M (2009) Learning sculpts the spontaneous activity of the resting human brain. *Proc Natl Acad Sci USA* 106(41):17558–17563.
18. Wang Z, et al. (2013) The relationship of anatomical and functional connectivity to resting-state connectivity in primate somatosensory cortex. *Neuron* 78(6):1116–1126.
19. Fries P, Reynolds JH, Rorie AE, Desimone R (2001) Modulation of oscillatory neuronal synchronization by selective visual attention. *Science* 291(5508):1560–1563.
20. Salinas E, Sejnowski TJ (2001) Correlated neuronal activity and the flow of neural information. *Nat Rev Neurosci* 2(8):539–550.
21. Fries P (2005) A mechanism for cognitive dynamics: Neuronal communication through neuronal coherence. *Trends Cogn Sci* 9(10):474–480.
22. Womelsdorf T, et al. (2007) Modulation of neuronal interactions through neuronal synchronization. *Science* 316(5831):1609–1612.
23. Fries P (2015) Rhythms for cognition: Communication through coherence. *Neuron* 88(1):220–235.
24. Bosman CA, et al. (2012) Attentional stimulus selection through selective synchronization between monkey visual areas. *Neuron* 75(5):875–888.
25. Gattass R, et al. (2005) Cortical visual areas in monkeys: Location, topography, connections, columns, plasticity and cortical dynamics. *Philos Trans R Soc Lond B Biol Sci* 360(1456):709–731.
26. Brewer AA, Press WA, Logothetis NK, Wandell BA (2002) Visual areas in macaque cortex measured using functional magnetic resonance imaging. *J Neurosci* 22(23): 10416–10426.
27. Gawne TJ, Richmond BJ (1993) How independent are the messages carried by adjacent inferior temporal cortical neurons? *J Neurosci* 13(7):2758–2771.
28. Miller JEK, Ayzenshtat I, Carrillo-Reid L, Yuste R (2014) Visual stimuli recruit intrinsically generated cortical ensembles. *Proc Natl Acad Sci USA* 111(38):E4053–E4061.
29. Sirota A, et al. (2008) Entrainment of neocortical neurons and gamma oscillations by the hippocampal theta rhythm. *Neuron* 60(4):683–697.
30. Buzsáki G (2006) *Rhythms of the Brain* (Oxford Univ Press, New York).
31. Roberts MJ, et al. (2013) Robust gamma coherence between macaque V1 and V2 by dynamic frequency matching. *Neuron* 78(3):523–536.
32. Vinck M, Womelsdorf T, Buffalo EA, Desimone R, Fries P (2013) Attentional modulation of cell-class-specific gamma-band synchronization in awake monkey area v4. *Neuron* 80(4):1077–1089.
33. Linkenkaer-Hansen K, Nikouline VV, Palva JM, Ilmoniemi RJ (2001) Long-range temporal correlations and scaling behavior in human brain oscillations. *J Neurosci* 21(4):1370–1377.
34. Freeman WJ (2004) Origin, structure, and role of background EEG activity. Part 1. Analytic amplitude. *Clin Neurophysiol* 115(9):2077–2088.
35. He BJ (2014) Scale-free brain activity: Past, present, and future. *Trends Cogn Sci* 18(9): 480–487.
36. Frien A, Eckhorn R, Bauer R, Woelbern T, Gabriel A (2000) Fast oscillations display sharper orientation tuning than slower components of the same recordings in striate cortex of the awake monkey. *Eur J Neurosci* 12(4):1453–1465.
37. Frien A, Eckhorn R (2000) Functional coupling shows stronger stimulus dependency for fast oscillations than for low-frequency components in striate cortex of awake monkey. *Eur J Neurosci* 12(4):1466–1478.
38. Belitski A, et al. (2008) Low-frequency local field potentials and spikes in primary visual cortex convey independent visual information. *J Neurosci* 28(22):5696–5709.
39. Womelsdorf T, et al. (2012) Orientation selectivity and noise correlation in awake monkey area V1 are modulated by the gamma cycle. *Proc Natl Acad Sci USA* 109(11): 4302–4307.
40. Grothe I, Neitzel SD, Mandon S, Kreiter AK (2012) Switching neuronal inputs by differential modulations of gamma-band phase-coherence. *J Neurosci* 32(46):16172–16180.
41. Bragin A, et al. (1995) Gamma (40-100 Hz) oscillation in the hippocampus of the behaving rat. *J Neurosci* 15(1 Pt 1):47–60.
42. Canolty RT, et al. (2006) High gamma power is phase-locked to theta oscillations in human neocortex. *Science* 313(5793):1626–1628.
43. Colgin LL, et al. (2009) Frequency of gamma oscillations routes flow of information in the hippocampus. *Nature* 462(7271):353–357.
44. Schomburg EW, et al. (2014) Theta phase segregation of input-specific gamma patterns in entorhinal-hippocampal networks. *Neuron* 84(2):470–485.
45. von Nicolai C, et al. (2014) Corticostriatal coordination through coherent phase-amplitude coupling. *J Neurosci* 34(17):5938–5948.
46. Arieli A, Sterkin A, Grinvald A, Aertsen A (1996) Dynamics of ongoing activity: Explanation of the large variability in evoked cortical responses. *Science* 273(5283):1868–1871.
47. Tsodyks M, Kenet T, Grinvald A, Arieli A (1999) Linking spontaneous activity of single cortical neurons and the underlying functional architecture. *Science* 286(5446): 1943–1946.
48. Engel AK, König P, Kreiter AK, Singer W (1991) Interhemispheric synchronization of oscillatory neuronal responses in cat visual cortex. *Science* 252(5009):1177–1179.
49. Bastos AM, et al. (2015) Visual areas exert feedforward and feedback influences through distinct frequency channels. *Neuron* 85(2):390–401.
50. Siegel M, Donner TH, Oostenveld R, Fries P, Engel AK (2008) Neuronal synchronization along the dorsal visual pathway reflects the focus of spatial attention. *Neuron* 60(4): 709–719.
51. Gregoriou GG, Gotts SJ, Zhou H, Desimone R (2009) High-frequency, long-range coupling between prefrontal and visual cortex during attention. *Science* 324(5931):1207–1210.
52. Nir Y, et al. (2008) Interhemispheric correlations of slow spontaneous neuronal fluctuations revealed in human sensory cortex. *Nat Neurosci* 11(9):1100–1108.
53. Logothetis NK, Pauls J, Augath M, Trinath T, Oeltermann A (2001) Neurophysiological investigation of the basis of the fMRI signal. *Nature* 412(6843):150–157.
54. Niessing J, et al. (2005) Hemodynamic signals correlate tightly with synchronized gamma oscillations. *Science* 309(5736):948–951.
55. Mukamel R, et al. (2005) Coupling between neuronal firing, field potentials, and FMRI in human auditory cortex. *Science* 309(5736):951–954.
56. Scheeringa R, et al. (2011) Neuronal dynamics underlying high- and low-frequency EEG oscillations contribute independently to the human BOLD signal. *Neuron* 69(3):572–583.
57. Schölvinck ML, Maier A, Ye FQ, Duyn JH, Leopold DA (2010) Neural basis of global resting-state fMRI activity. *Proc Natl Acad Sci USA* 107(22):10238–10243.
58. Gray CM, König P, Engel AK, Singer W (1989) Oscillatory responses in cat visual cortex exhibit inter-columnar synchronization which reflects global stimulus properties. *Nature* 338(6213):334–337.
59. Eckhorn R, et al. (1988) Coherent oscillations: A mechanism of feature linking in the visual cortex? Multiple electrode and correlation analyses in the cat. *Biol Cybern* 60(2):121–130.
60. Einevoll GT, Kayser C, Logothetis NK, Panzeri S (2013) Modelling and analysis of local field potentials for studying the function of cortical circuits. *Nat Rev Neurosci* 14(11):770–785.
61. Miller KJ, Sorensen LB, Ojemann JG, den Nijs M (2009) Power-law scaling in the brain surface electric potential. *PLOS Comput Biol* 5(12):e1000609.
62. Ray S, Maunsell JHR (2011) Different origins of gamma rhythm and high-gamma activity in macaque visual cortex. *PLoS Biol* 9(4):e1000610.
63. He BJ, Snyder AZ, Zempel JM, Smyth MD, Raichle ME (2008) Electrophysiological correlates of the brain's intrinsic large-scale functional architecture. *Proc Natl Acad Sci USA* 105(41):16039–16044.
64. Mantini D, Perrucci MG, Del Gratta C, Romani GL, Corbetta M (2007) Electrophysiological signatures of resting state networks in the human brain. *Proc Natl Acad Sci USA* 104(32):13170–13175.
65. Laufs H, et al. (2003) EEG-correlated fMRI of human alpha activity. *Neuroimage* 19(4): 1463–1476.
66. Laufs H, et al. (2003) Electroencephalographic signatures of attentional and cognitive default modes in spontaneous brain activity fluctuations at rest. *Proc Natl Acad Sci USA* 100(19):11053–11058.
67. Hipp JF, Hawellek DJ, Corbetta M, Siegel M, Engel AK (2012) Large-scale cortical correlation structure of spontaneous oscillatory activity. *Nat Neurosci* 15(6):884–890.
68. Hawellek DJ, et al. (2013) Altered intrinsic neuronal interactions in the visual cortex of the blind. *J Neurosci* 33(43):17072–17080.
69. de Pasquale F, et al. (2010) Temporal dynamics of spontaneous MEG activity in brain networks. *Proc Natl Acad Sci USA* 107(13):6040–6045.
70. Popa D, Popescu AT, Paré D (2009) Contrasting activity profile of two distributed cortical networks as a function of attentional demands. *J Neurosci* 29(4):1191–1201.
71. He BJ, Zempel JM, Snyder AZ, Raichle ME (2010) The temporal structures and functional significance of scale-free brain activity. *Neuron* 66(3):353–369.
72. Oostenveld R, Fries P, Maris E, Schoffelen J-MM (2011) FieldTrip: Open source software for advanced analysis of MEG, EEG, and invasive electrophysiological data. *Comput Intell Neurosci* 2011(1):156869.
73. Mitra PP, Pesaran B (1999) Analysis of dynamic brain imaging data. *Biophys J* 76(2): 691–708.
74. Dhamala M, Rangarajan G, Ding M (2008) Estimating Granger causality from fourier and wavelet transforms of time series data. *Phys Rev Lett* 100(1):018701.
75. Van Essen DC, Glasser MF, Dierker DL, Harwell J (2012) Cortical parcellations of the macaque monkey analyzed on surface-based atlases. *Cereb Cortex* 22(10): 2227–2240.